Optimization of Polypropylene/Clay Nanocomposite Processing Using Box-Behnken Statistical Design

Saikat Banerjee,[1] Mangala Joshi,[2] Anup K. Ghosh[1]

[1]*Centre for Polymer Science and Engineering, Indian Institute of Technology Delhi, New Delhi 110016, India*
[2]*Department of Textile Technology, Indian Institute of Technology Delhi, New Delhi 10016, India*

Received 23 June 2010; accepted 25 March 2011
DOI 10.1002/app.34566
Published online 23 August 2011 in Wiley Online Library (wileyonlinelibrary.com).

ABSTRACT: A wide range of process parameters regulate the final morphology achieved in layered silicate based polymer nanocomposites. This study deals with the optimization of process variables to improve the matrix formulation. A three-factor, three-level Box-Behnken design with compatibilizer concentration (X_1), clay concentration (X_2), and screw speed (X_3) as the independent variables were selected for the study. The dependent variable was mechanical property of the final nanocomposites. Maleic anhydride grafted polypropylene (PP-*g*-MA) compatibilizer and organoclay (Cloisite 15A) was melt blended with polypropylene separately in a corotating twin screw extruder. The clay was modified with fluorescent dye Nile Blue A Perchlorate (NB) and the adsorbed dye content in the clay gallery was estimated by using UV-spectrophotometric method. The Minitab-15 software was used for analysis of the results obtained. Optimum compositions for better dispersion were achieved from contour plots and response surface methodology. It was supported by a unique fluorescence spectrophotometry along with transmission electron microscopy and X-ray diffraction technique. An intensity ratio close to unity showed a better exfoliated morphology. © 2011 Wiley Periodicals, Inc. J Appl Polym Sci 123: 2042–2051, 2012

Key words: clay-nanocomposite; process optimization; fluorescence spectrophotometry; X-ray diffraction

INTRODUCTION

Melt processing of polymer/clay nanocomposites result in morphology development like tactoids, intercalated or a combination of intercalation and exfoliation.[1,2] The morphology depends on factors like shear during mixing, diffusion of polymer chains into the clay gallery and the interaction of hydrophobic polymer with the hydrophilic clay surface. Because of the difference in polarity of polypropylene (PP) and organoclay, it is difficult to obtain PP/nanoclay composites with exfoliated structure of the filler in the PP matrix during extrusion process.[3] To improve the dispersion of clay in PP matrix, functional oligomers like maleic anhydride grafted PP (PP-*g*-MA) with a specific grafting has been used as a compatibilizer. The interaction is enhanced by a strong hydrogen bonding between —COOH groups of the compatibilizer and the free Si—OH groups of silicate layers.[4] But a higher content of compatibilizer and clay is detrimental to the mechanical properties of the final composite beyond which reagglomeration of clay platelets takes place and causes no further enhancement in mechanical properties. Thus, the aim should be to optimize the parameters related to processing conditions (screw speed, i.e., shear) as well as the composition (clay and compatibilizer content) for PP-based nanocomposites.[5–7]

In case of multivariate system, changing of dependable variables at a time and to study their effects on the response is a complicated labor intensive technique. Design of experiments (DOE) is a statistical technique for optimizing such multivariable systems. Using DOE based on response surface methodology,[8] optimum composition can be achieved with a minimum number of experiments without the need for studying all possible combinations experimentally. This design and analysis of experiments, tries to relate a response or output variable to the input variables that affect it. It shows the direction in which one should move to change the input levels as to decrease or increase the response.[9–11]

Box-Behnken statistical design for optimization has been carried out in fields like biotechnology,[12–15] textile application for yarn manufacturing,[16] polymeric blown film,[17] and fluid dynamics,[18] but very rare application has been found in case of polymeric nanocomposite processing. The goal of this study is to determine the optimized concentration of PP-*g*-MA compatibilizer and the organically modified

Correspondence to: A. K. Ghosh (anupkghosh@gmail.com).

Contract grant sponsors: Department of Science and Technology, Government of India, and Reliance Industries Ltd., India

clay as well as the screw rpm for appropriate morphology development during melt compounding of polymer–clay nanocomposite in a corotating twin screw extruder. The response surface methodology was applied using a Box and Behnken experimental design for the purpose. The Box-Behnken experimental design optimizes the number of experiments to be carried out to ascertain the possible interactions between the parameters studied and their effects. The design consists of a central point and the middle points of the edges of the cube confined on the sphere.[19] It is a three-level fractional factorial design that allows prediction of the combined effects of three controlled factors of 15 sets of test conditions and three central points. Three levels were attributed to each factor, coded as −1 (low), 0 (medium), and +1 (high). The mathematical relationship between the three variables and the response can be expressed by the second order polynomial equation:

$$Y = \beta_0 + \beta_1 X_1 + \beta_2 X_2 + \beta_3 X_3 + \beta_{11} X_{12} + \beta_{22} X_{22} + \beta_{33} X_{32} + \beta_{12} X_1 X_2 + \beta_{13} X_1 X_3 + \beta_{23} X_2 X_3 \quad (1)$$

where, Y is the response; β_0 is a constant; β_1, β_2, β_3 are linear coefficients; β_{11}, β_{22}, β_{33} are quadratic coefficients, and β_{12}, β_{13}, β_{23} are cross-product coefficient. X_1, X_2, and X_3 are the factors to be studied. In this article, a method based on the fluorescence spectroscopy was performed to study the dispersion of clay and the clay/polymer interfaces. The approach has been made on the basis of previous studies on the absorption and emission spectra of fluorescent dyes exchanged and attached into clay gallery.[20–26] X-ray diffraction (XRD) analysis and transmission electron microscopy (TEM) were performed as supportive tool for examining the crystal structure and morphology of polymer/clay nanocomposites. A change in peak position indicated the morphology whether it is intercalated and/or exfoliated.[27–29] The microstructure of polymer–clay nanocomposite is directly related to the dispersion of clay platelets in the polymer matrix, which reflects as change in mechanical properties. This investigation was carried out to maximize the mechanical properties by optimizing the right combination of the individual variables like compatibilizer content, clay content, and shear (screw speed).

EXPERIMENTAL

Materials

The isotactic polypropylene (iPP, REPOL H110 MA, MFI∼ 11) used in this study was commercially available from Reliance Industries, India. Maleic anhydride-grafted polypropylene (PP-*g*-MA, Fusabond PMD 511D) with a melt flow index of 24 at 190°C and 2.16 kg load was purchased from Du Pont Ltd. The clay, Cloisite 15A, modified with dimethyl, hydrogenated tallow and quaternary ammonium was purchased from Southern Clay Products, which has a cation exchange capacity of 125 mEq/100 g. The clay was further modified with cationic fluorescent dye Nile Blue A Perchlorate (NB) (Fig. 1) (M.P ∼ 290°C, λ_{max} ∼ 628 nm, 95% dye content) using a secondary ion exchange process. The dye was procured from Sigma Aldrich, India.

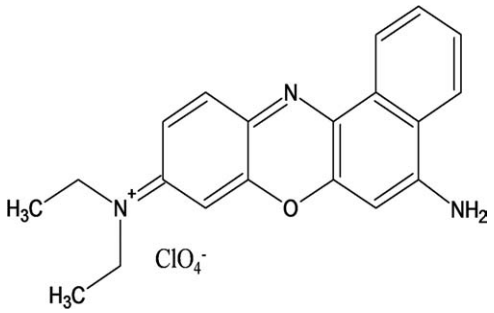

Figure 1 Chemical structure of Nile Blue A Perchlorate, a fluorescent dye.

Modification of organoclay with dye

The clay was modified with NB using a secondary ion exchange method. The procedure followed was similar to that described in our previous article for methylene blue dye.[30] A measured amount of NB and Cloisite 15A were taken to achieve complete ion exchange. Nile blue was dissolved in hot ethanol and to this solution the organoclay was added continuously with rapid stirring. The volume was adjusted with distilled water and heated at 70°C for 1 h for secondary ion exchange. The slurry was allowed to stand in a dark place for 3–4 days to reach equilibrium and then filtered. The residue was washed thoroughly with 50% hot ethanol until the filtrate was colorless. Finally, the modified clay was dried in vacuum oven at 80°C for 24 h and ground. The filtrate was collected and amount of dye exchanged to clay gallery was estimated by using UV-spectrophotometric method.

Nanocomposite processing

To optimize the composition and process parameters a three-factor Box-Behnken model was used. The minimum and maximum level of each factor (PP-*g*-MA, clay, and screw rpm) was fed into Minitab-15 software. It produced fifteen combinations. The melt mixing was done in a Prism Eurolab-16 corotating twin screw extruder having a high shear screw configuration for better mixing. The screws contain kneading blocks with 30°stagger angle. Each

TABLE I
Temperature Profile During Extrusion Process

Barrel zone	Zone 1	Zone 2	Zone 3	Zone 4	Zone 5	Zone 6	Zone 7	Zone 8	Zone 9	Zone 10
Temperature (°C)	165	170	175	180	185	190	195	200	205	210

kneading block consists of seven discs with $L = 0.25D$, where L is the disc length and D is the diameter. The processing temperature profile from feed to die zone (Table I) was selected such as to ensure proper melt viscosity for the mixing while at the same time minimizing degradation of both the polymer and dye. Before melt processing, all the components were dried at 80°C for 24 h. During processing a particular feed rate was maintained.

The extruded strands were chopped and injection molded using L and T Demag PFY40 machine at 200°C for mechanical testing. The results were again fed into the software to obtain surface and contour plots.

Characterization techniques

Wide angle X-ray scattering (WAXS) patterns for organically modified clay and dyed clay were recorded by using Cu Kα radiation (40 kV, 30 mA) generated by an X-ray diffractometer (Philips X'Pert PRO); corresponding data were scanned in the reflection mode over a 2θ-angle of 2°–10° to characterize the inter layer spacing (*d*-spacing) of the dyed MMT after compounding. The scanning rate was 0.01°/s.

Tensile tests were performed at room temperature according to ASTM D638, using Zwick Z010 at a testing rate of 50 mm/min. Flexural tests were also done according to ASTM D790 using the same instrument. Notched Izod impact strength was measured using IMPats Faar-15 impact tester with a 2 J hammer at room temperature (ASTM D256). An average of five tests of each specimen was reported.

The fluorescence spectrophotometric study of the compression molded disc samples was carried out using Fluorolog Horibajobin Yvon spectrophotometer. Xenon-arc lamp was the source. The samples were excited using a "2, 1" slit at a wavelength of 407 nm. For emission spectra, a wavelength range of 420–750 nm was selected.

For TEM freshly cut glass knives with cutting edge of 45° were used to get the cryosections of 50-nm thickness by using a Leica Ultracut UCT microtome. JEOL-2100 electron microscope (Tokyo, Japan) having LaB6 filament and operating at an accelerating voltage of 200 kV was utilized to obtain the bright field images of the cryo-microtomed samples.

RESULTS AND DISCUSSION

UV-spectrophotometric study

The amount of dye adsorbed inside the clay gallery was determined using UV-spectrometric technique. The absorbance of NB solution having five different known concentrations was measured using 1 nm slit. A concentration (mmol) versus absorbance (A) calibration curve was plotted. A Perkin–Elmer Lambda-25 UV/VIS spectrometer was used for this purpose. The concentration of the NB dye in the filtrate was estimated by measuring the absorbance and corresponding concentration reading in the calibration curve (Fig. 2). It was found that, the adsorbed dye concentration in the clay gallery was 2.106×10^{-5} mol/g of clay.

Experimental design

Three experimental factors, PP-*g*-MA compatibilizer (wt %), clay (wt %), and screw speed (rpm) were varied at three levels: minimum, intermediate, and maximum. These factors were chosen as they are considered to have the most significant effect on the clay dispersion and exfoliation during melt processing. The levels were chosen from the knowledge based on the initial experimental trials and shown in Table II. In these studies, three most significant response factors: tensile modulus, flexural modulus, and impact strength were introduced to determine the optimum conditions. The inclusion of these three center points provided a more precise estimation of experimental error and provided a measure for the

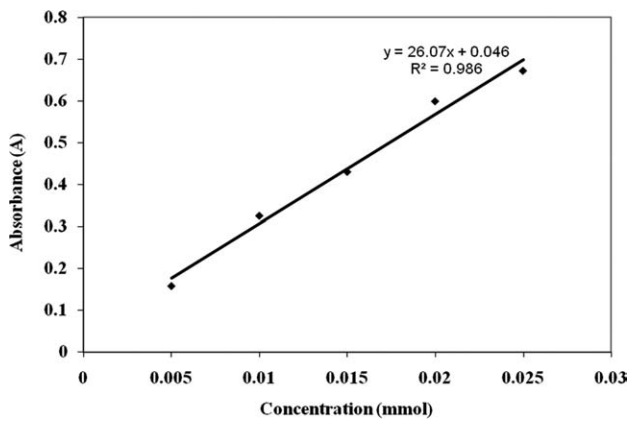

Figure 2 Calibration curve of the filtrate after clay modification with Nile Blue A Perchlorate dye.

TABLE II
The Variables and Their Levels used in Box-Behnken Design

Factors	Low (−1)	Medium (0)	High (+1)
PP-*g*-MA (wt %)	0.50	4.25	8.00
Organoclay (wt %)	0.50	2.25	4.00
Screw speed (rpm)	100	300	500

adequacy of the model.[31] Box-Behnken DOE for the three variables were done and mechanical properties (response) for the 15 statistically designed combinations were determined experimentally (Table III). The results of the experimental design were studied and interpreted by Minitab-15 statistical software to estimate the response of the dependent variable.

Equation for uncoded samples:

$$Y_1 = 391.288 - 8.67527X_1 - 9.91067X_2 - 0.221679X_3 - 0.1464X_1^2 + 0.0379592X_2^2 + 0.000423344X_3^2 + 2.184X_1X_2 + 0.0105533X_1X_3 + 0.00294286X_2X_3 \quad (2)$$

$$Y_2 = 1301.37 + 50.2764X_1 + 103.964X_2 + 0.146784X_3 - 4.54308X_1^2 - 12.7109X_2^2 - 0.000193823X_3^2 - 9.37714X_1X_2 + 0.0114833X_1X_3 - 0.0684643X_2X_3 \quad (3)$$

$$Y_3 = 20.0242 + 2.58358X_1 + 1.24767X_2 + 0.106954X_3 - 0.208119X_1^2 + 0.103946X_2^2 - (3.54167E - 06)X_3^2 0.105143X_1X^2 - 0.00198X_1X^3 - 0.00178571X_2X_3 \quad (4)$$

where Y_1 = tensile modulus (MPa), Y_2 = flexural modulus (MPa), Y_3 = impact strength (J/m), X_1 = PP-*g*-MA (wt %), X_2 = clay (wt %), X_3 = speed (rpm).

In eqs. (2)–(4), synergistic effect is expressed by positive sign whereas negative sign corresponds to antagonistic effect. The critical points were obtained by solving these equation systems formed by the partial derivatives of the functions.

To optimize the variable concentration, a comparative representation of mechanical properties of the different (composition 1–15) melts processed PP/clay nanocomposites is shown in Table III. A close approach of the observed and predicted value of response shows the effectiveness of the model (Table IV).

Morphological analysis

Figure 3 shows the fluorescence spectra of Cloisite 15A, NB, a cationic dye and the dye modified Cloisite 15A clay. The emission spectra were obtained at room temperature when excited at a wavelength of 407 nm for better spectra.[21] Figure 3(a) shows a smaller emission peak of Cloisite 15A at 668 nm wavelength. This insignificant emission peak may arise due to presence of sodium and other cations inside the clay gallery in small amount.[32] For alcoholic solution of the dye, the characteristic intensity maxima of the dye is observed at 680 nm [Fig. 3(b)], whereas the characteristic emission intensity peaks of the dyed clay were observed near 555 nm and 625 nm [Fig. 3(c)]. The peak at 555 nm arises due to the presence of exchanged dye inside the clay gallery and the 625 nm peak comes from the dispersed dye. Since the gallery spacing of the clays is not sufficient enough to accommodate all the dye, so various types of dye adduct (H-adducts, J-adducts) are formed in

TABLE III
Experimental Parameters and Response Values for Process Optimization by Box–Behnken Design

Compositions (with code)	PP-*g*-MA (wt %)	Clay (wt %)	Speed (rpm)	Tensile modulus (MPa)	Flexural modulus (MPa)	Impact strength (J/m)
1(R_1)	4.25	2.25	300	376 ± 39.0	1540 ± 40.1	27
2 (R_2)	0.50	2.25	500	364 ± 33.9	1501 ± 17.9	24
3 (R_3)	0.50	2.25	100	338 ± 52.9	1411 ± 13.1	24
4 (R_4)	8.00	2.25	500	383 ± 47.4	1579 ± 30.3	25
5 (R_5)	4.25	4.00	100	331 ± 48.4	1531 ± 57.3	32
6 (R_6)	8.00	0.50	300	294 ± 51.2	1478 ± 29.5	25
7 (R_7)	8.00	4.00	300	346 ± 56.6	1250 ± 25.2	23
8 (R_8)	8.00	2.25	100	325 ± 44.0	1455 ± 21.7	30
9 (R_9)	4.25	0.50	100	353 ± 66.6	1472 ± 23.9	26
10 (R_{10})	4.25	2.25	300	348 ± 41.2	1533 ± 33.1	31
11 (R_{11})	0.50	4.00	300	349 ± 31.3	1524 ± 44.6	28
12 (R_{12})	4.25	2.25	300	288 ± 90.7	1555 ± 45.0	28
13 (R_{13})	4.25	4.00	500	358 ± 58.5	1503 ± 32.0	30
14 (R_{14})	0.50	0.50	300	354 ± 51.3	1507 ± 24.9	27
15 (R_{15})	4.25	0.50	500	312 ± 51.3	1525 ± 43.2	28

TABLE IV
The Observed and Predicted Response of the Three Variables using Box-Behnken Design

Composition number	Tensile modulus (MPa)		Composition number	Tensile modulus (MPa)		Composition number	Tensile modulus (MPa)	
	Observed	Predicted		Observed	Predicted		Observed	Predicted
1	376	338	6	294	314	11	349	333
2	364	368	7	346	343	12	288	337
3	338	350	8	325	321	13	358	373
4	383	370	9	353	338	14	354	356
5	331	337	10	348	338	15	312	359

this restricted space. As a result, shifting of the emission maxima occurs toward lower side of wavelength region (blue shift) in comparison with the dye alone.

A comparative study of fluorescence spectrum for different compositions is shown in Figure 4. It is evident that both peak intensities (I_{555} and I_{625}) and peak positions change with the compositions with respect to wavelength [Fig. 4(a)]. If we consider the compositions 2 and 3 (referred as R_2 and R_3, respectively, in Table III), both are composed of 0.5 wt % PP-*g*-MA and 2.25 wt % dyed clay, but different in screw rpm. Composition R_2 is exposed to more shear (at 500 rpm) than composition R_3 (at 100 rpm). It is also reflected in the spectra. As R_2 is more exposed to shear, more peeling out of the clay layers impels the polymer chains to diffuse inside the clay gallery by partially replacing the exchanged dye molecules. This reduction in dye concentration inside clay gallery causes a decrease in the intensity of the fluorescence spectra (I_{555}) at the characteristic 529 nm wavelength to 1.27E + 5.0 cps (for R_2) from 1.97E + 5.0 cps (for R_3). As the matrix is non- polar in nature (PP matrix) and contains very less amount of polar PP-*g*-MA compatibilizer, it becomes less compatible with the polar cationic dye molecules. As a result, the replaced dye molecules interact with each other to form dimer, oligomer type of aggregates in that polymer matrix. This aggregation reduces the intensity of the emission spectra (I_{625}) in the matrix from 1.01E + 5.0 cps (for R_3) to 0.87E + 5.0 cps (for R_2) and known as concentration quenching. Since due to more shear, the polymer chains in composition 2 diffuse more inside the clay gallery, therefore it can be said that composition 2 has better exfoliated morphology than composition 3. It is also

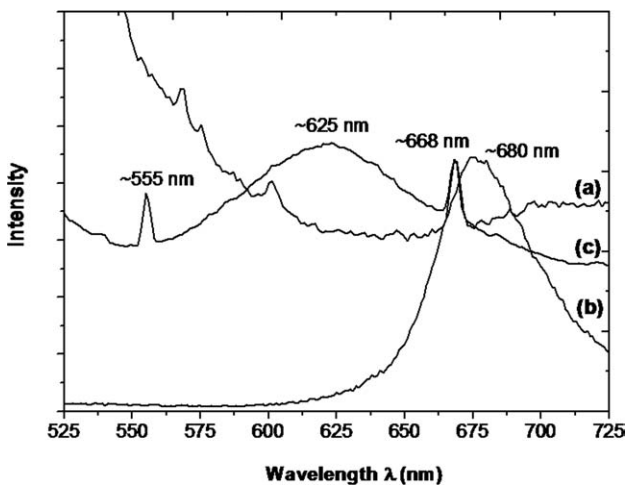

Figure 3 Fluorescence spectra of: (a) Cloisite 15A, (b) alcoholic solution of Nile Blue A Perchlorate, and (c) Nile Blue A Perchlorate modified Cloisite 15A.

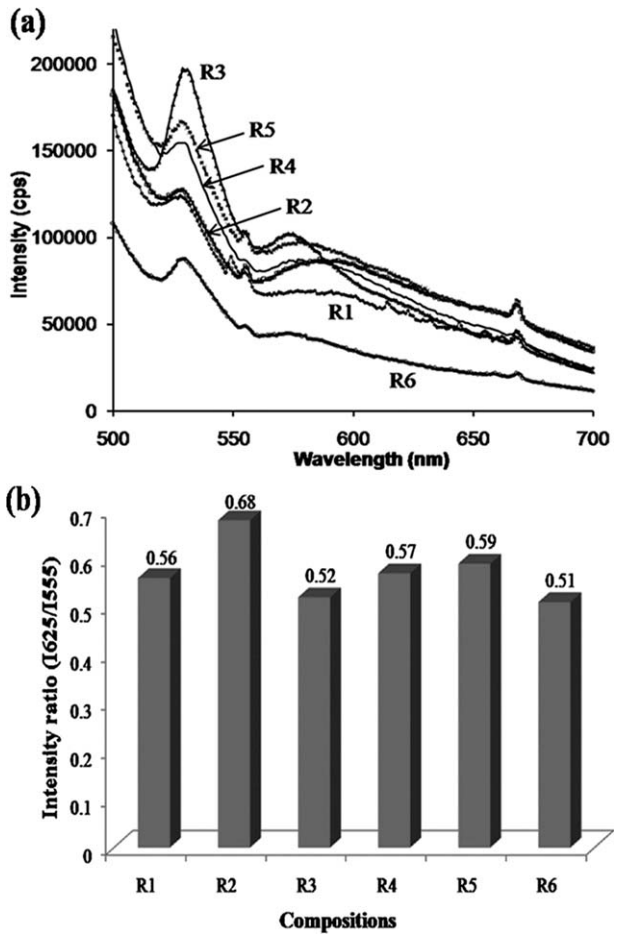

Figure 4 (a) Fluorescence spectra and (b) Intensity ratio of compounded polypropylene with PP-*g*-MA and dyed clay.

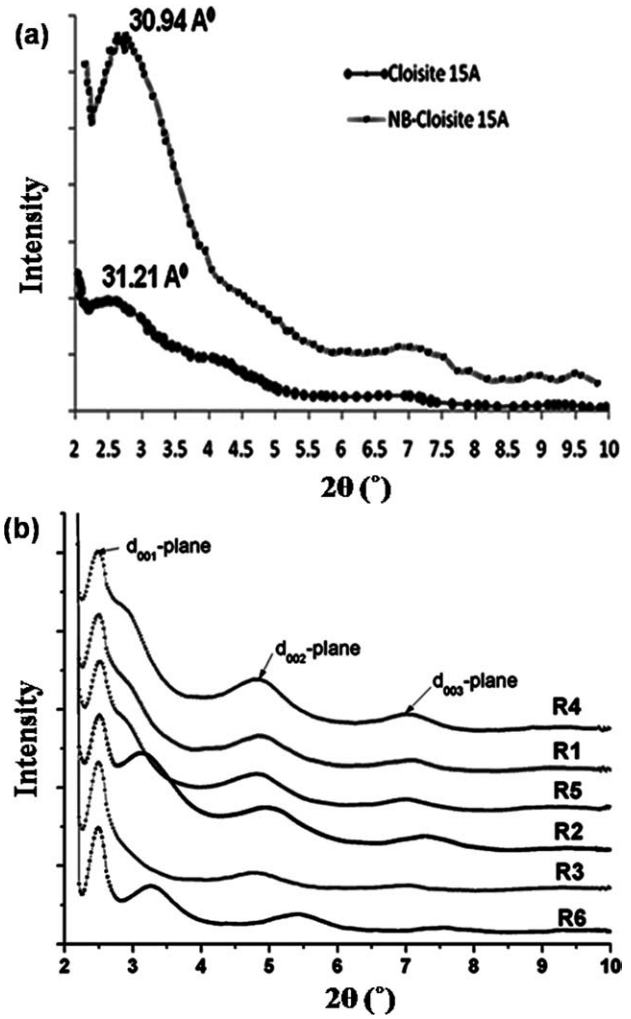

Figure 5 WAXD pattern for: (a) Cloisite 15A and Nile Blue A Perchlorate modified Cloisite 15A and (b) compositions with varying PP-*g*-MA, clay concentration (wt %) and screw rpm.

supported by the intensity ratio (I_{625}/I_{555}) column shown in Figure 4(b). As more and more the clays are exfoliated, the intensity ratio approaches toward higher value. Composition 2 shows a higher intensity ratio of 0.68 than 0.52 of composition 3. This ratio favors the more exfoliated morphology of composition 2. Figure 4(b) also shows an intensity ratio of 0.59 for composition 5 (designated as R_5) which is higher than 0.52 for composition 3, i.e., exfoliation is more for R_5 than R_3. In both the cases, shear is same (processed at same 100 rpm), but here dominating factor is compatibilizer to clay ratio. Higher is the ratio (R_5 composition), more is the dispersion and/or exfoliation.

Figure 5(a) shows the X-ray diffractograms of the organically modified clay Cloisite 15A and the dyed clay. In the shoulder-shaped spectrum the interlayer distance (d_{001}-peak) was calculated from the point where the inflection rate reaches a maximum. The basal spacing (d_{001}-plane) for Cloisite 15A comes around 31.2 Å, whereas for dyed clay it is around 30.9 Å. This narrow decrease in *d*-spacing is due to the fact that, during secondary ion exchange some of the bulkier organic modifier with long chain tallow inside the clay gallery is replaced by planar Nile blue dye molecules. With the application of shear, polymer chains can easily diffuse into the clay gallery creating an intercalated morphology which is supported by a narrow increase in *d*-spacing from 30.9 A°. The higher *d*-spacing value in composition R_2 as compared with R_3 indicates better intercalated/exfoliated morphology [Fig. 5(b)]. Presence of compatibilizer also plays an important role for intercalation and exfoliation. An increase in compatibilizer to clay ratio promotes the diffusion of polymer chains into the gallery. A rise in both tensile modulus (Table III) and intensity ratio [Fig. 4(b)] also corroborates the fact.

Figure 6 shows the TEM images of PP/clay nanocomposites at 12kX magnifications and processed at various screw speed keeping compatibilizer and clay content fixed at 0.50 wt % and 2.25 wt %, respectively. The dark layers represent the clay layers. It is found that nanocomposites processed at higher screw rpm (composition R_2, 500 rpm) experienced more shear than composition R_3 processed at 100 rpm. Presence of well intercalated/exfoliated morphology in case of composition R_2 [Fig. 6(b)] supports the influence of shear on dispersion.

Response surface regression analysis

The responses at any regime in the interval of our experiment design could be calculated from eqs. (2) to (4).

Optimization calculations

Tensile modulus

The surface contour plots show the effect of process parameters on mechanical properties of the final composite. Figure 7 shows how tensile modulus depends upon the process parameters like screw speed (rpm), clay concentration (wt %) and concentration of the compatibilizer PP-*g*-MA (wt %). The tensile strength and modulus generally tend to increase with an increase in clay content and the trend is more prominent for the tensile modulus. The tensile modulus increases both with screw speed and clay concentration at a particular compatibilizer concentration (4.25 wt %) [Fig. 7(a)], but in case of compatibilizer concentration it increases upto a certain level and then rapidly decreases. The improvement in mechanical property mainly depends upon the polymer to filler interaction, so that the stress can easily be transferred from the

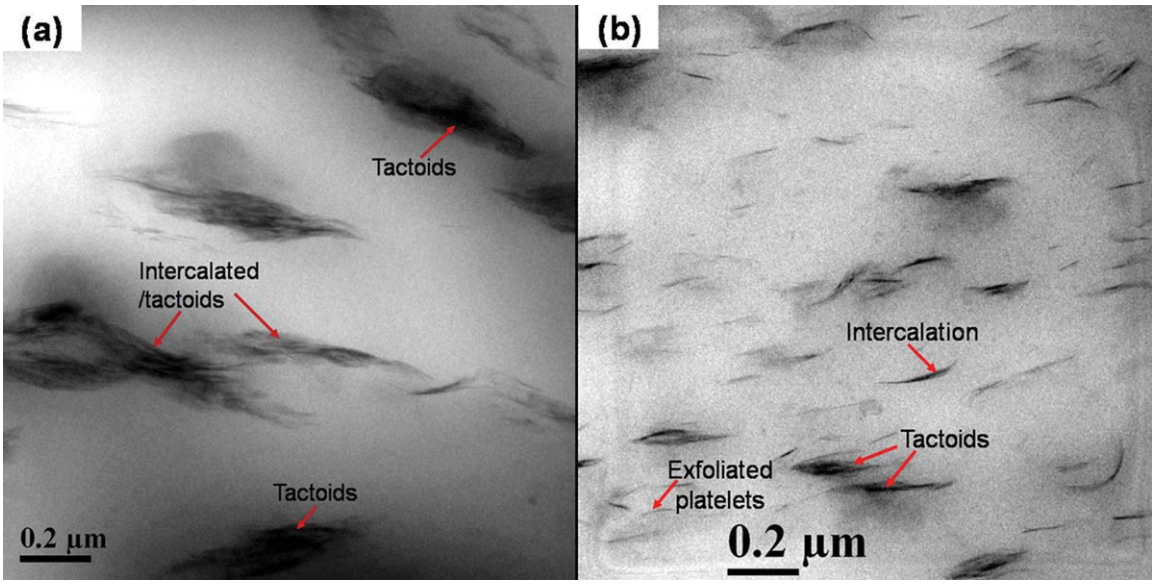

Figure 6 TEM images of PP/clay nanocomposites processed at different screw rpm: (a) 100 rpm (R_3) and (b) 500 rpm (R_2) (×12,000 magnification). [Color figure can be viewed in the online issue, which is available at wileyonlinelibrary.com.]

polymer matrix to the reinforcing filler surface. The tensile modulus shows better improvement at low clay content, indicating that the clay layers are better exfoliated at this level. With an increase in clay concentration, more filler surfaces are exposed to the matrix for better transfer of stress. But after a certain limit when the filler to matrix ratio crosses the critical level (>4 wt % clay), further addition of clay leads to a reduction in tensile ductility.[33] At this level, the clay platelets commence to get stacked and agglomerated once again. As a result, the exposed surface area does not further increase with more clay added and a dramatic decrease in tensile modulus is observed.[34] Figure 7(a) also shows that tensile modulus increases with screw rpm. The clays are initially in large tactoid form, so with increase in

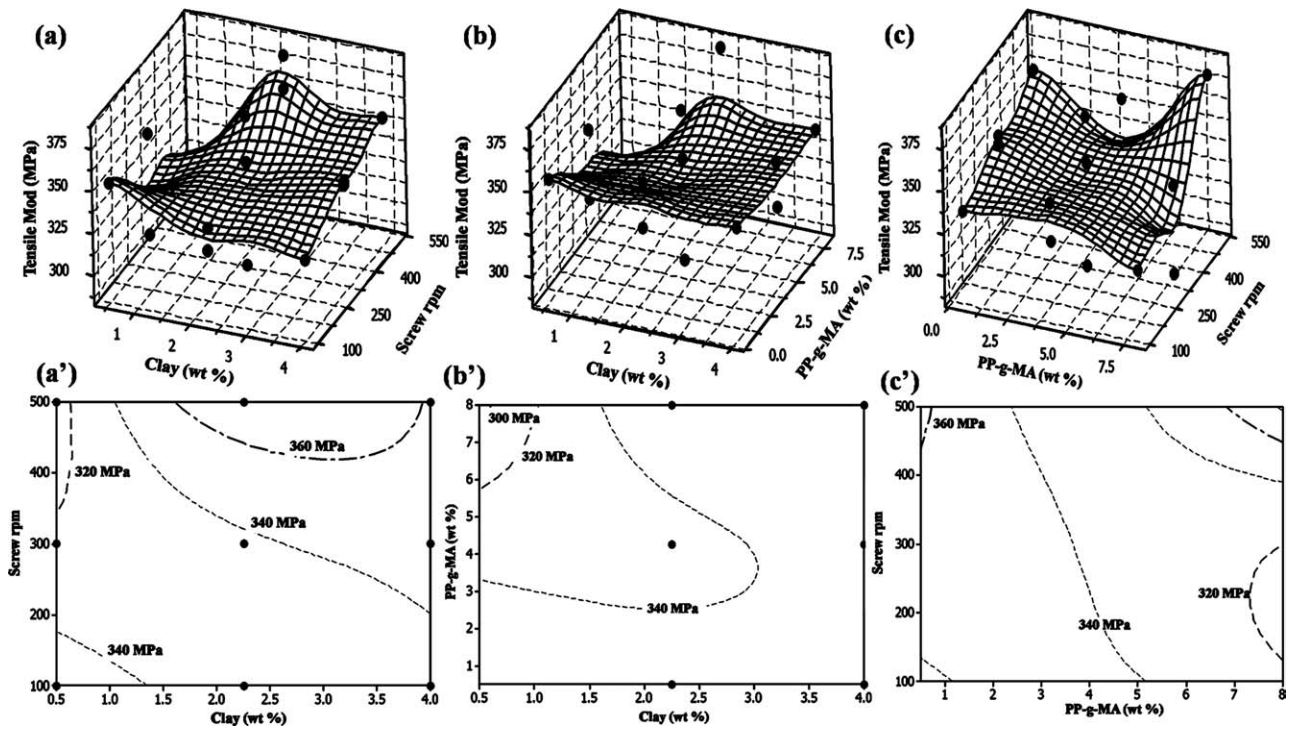

Figure 7 Diagrams (a, a′ to c, c′) showing the surface and contour plots for the three variables on the tensile modulus (MPa).

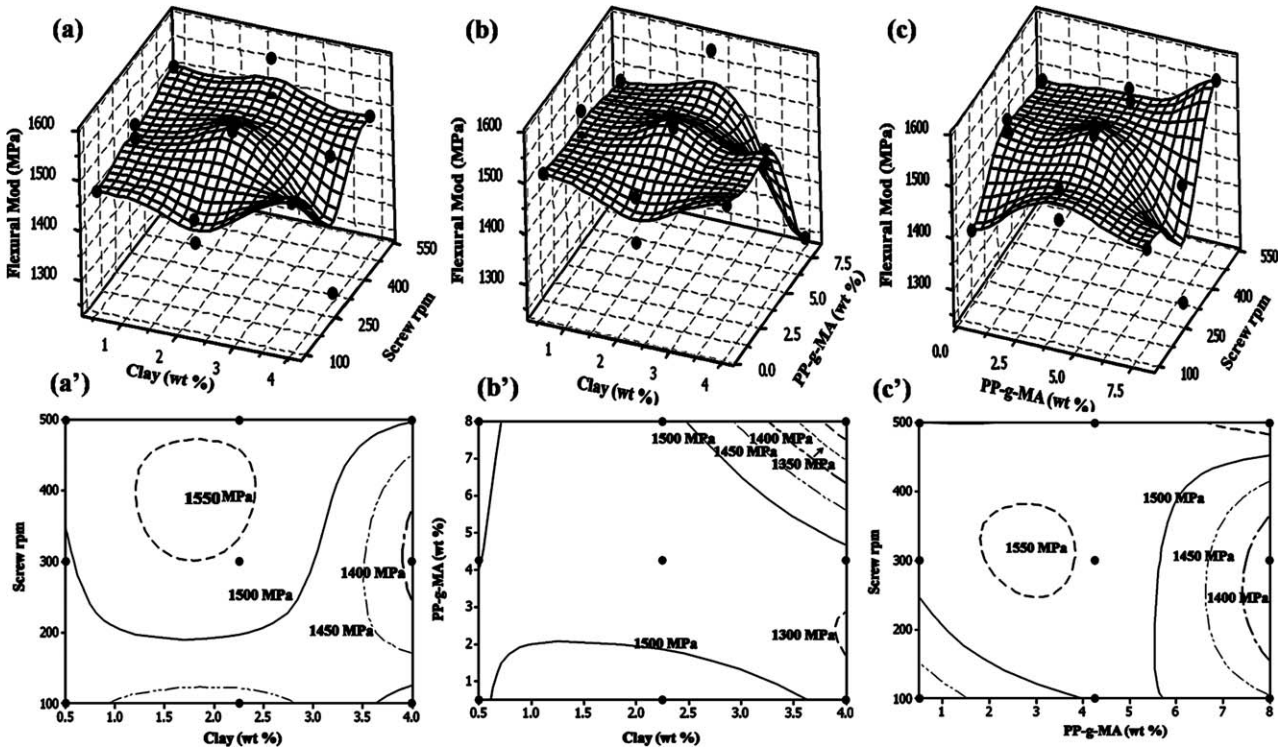

Figure 8 Diagrams (a, a′ to c, c′) showing the surface and contour plots for the three variables on the flexural modulus (MPa).

rpm it experiences more shear and size reduction occurs. This causes an increase in available surface area. With more shear the clays move from intercalated to exfoliated structure where the clay surfaces are exposed to their maximum level. It results in maximum polymer to clay interaction, i.e., tensile modulus to its maximum value. Beyond that shear ($\sim$ 400 rpm), there is no significant change in clay morphology. Since organophilic PP is less prone to be compatible with organophobic layered silicate, so a compatibilizer PP-*g*-MA is needed. With increase in compatibilizer concentration, more polymer chains are capable for intercalation to the clay gallery. More intercalation exposes more clay surfaces for stress transfer from the matrix to the reinforcement, which results an increase in the modulus. But further increase in compatibilizer concentration reduces the mechanical property as the higher molecular weight PP is been replaced by comparatively low molecular weight compatibilizer. Figure 7(b) shows a reduction in modulus after a critical concentration of PP-*g*-MA (i.e., $\sim$ 4.25 wt %). So, it may be concluded that at a particular screw speed of 300 rpm the optimum composition range lies in between 2 and 4 wt % for clay and less than 5 wt % for compatibilizer. A compatibilizer content above 5 wt % may hamper the mechanical properties of the final composites.

Flexural modulus

Figure 8 shows the effect of clay, compatibilizer, and screw rpm on flexural property. At a fixed compatibilizer concentration (4.25 wt %), flexural modulus increases with an increase in clay concentration upto a level of about 2.5 wt % beyond which there in no significant change [Fig. 8(a,a′)]. This observation suggests that the interfacial interaction between the clay surface and polymer matrix plays an important role in determining flexural modulus also. The available surface area for polymer clay interaction increases with an increase in clay amount from 1.23 to 2.43 wt % (optimum range) and beyond this limit addition of clay leads to more agglomerated/tactoid morphology which reflects in a decreasing flexural modulus trend. The screw speed below 300 rpm is also not sufficient to create shear for better intercalation and exfoliation. The contour plot [Fig. 8(a′)] shows that flexural modulus is significantly increased ($\sim$ 1550 MPa) at the screw rpm of about 300–472.

At a constant shear (at 300 rpm), a better result in flexural modulus (MPa) can be seen below the clay concentration of 3.5 wt % and a compatibilizer concentration of 5 wt % [Fig. 8(b,b′)]. If clay concentration is maintained at an intermediate value of 2.25 wt %, it is clear from both the plots [Fig. 8(c,c′)], the optimized value for screw speed and compatibilizer

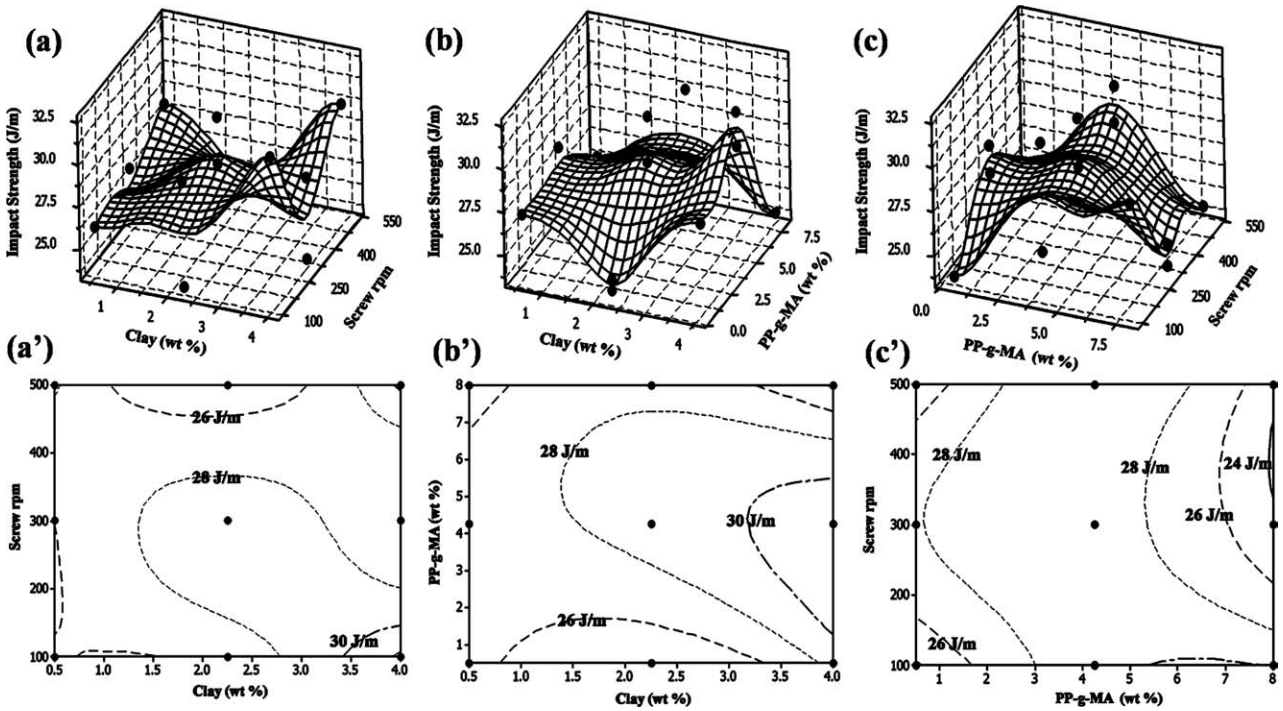

Figure 9 Diagrams (a, a′ to c, c′) showing the surface and contour plots for the three variables on the impact strength (J/m).

PP-*g*-MA are in between the range of 245–380 rpm and 1.9–3.8 wt %, respectively. At a particular screw speed (300 rpm) optimum level for clay shows in between 1.5 and 2.5 wt % [Fig. 8(a′)] and that for PP-*g*-MA compatibilizer it lies in between 2 and 4 wt % [Fig. 8(c′)].

Impact strength

In the case of thermoplastic polymers, the addition of clay generally enhances their tensile modulus and strength. However, impact toughness of nanocomposite depends on the extent of clay dispersion in the amorphous region of the thermoplastics.[35–37] It seems to be that, exfoliated clay platelets dispersed in melt compounded thermoplastic matrix can hinder the crack propagation resulting in an increase in impact properties.[38] At a compatibilizer concentration of 4.25 wt %, impact strength is optimum ($\sim$ 28 J/m) when the clay level is in the range of 1.5 to 3.0 wt % and 300 rpm screw speed [Fig. 9(a,a′)]. But if a clay concentration of 2.25 wt % is considered, the optimum value of impact strength (28 J/m) reaches at a compatibilizer concentration of 3.0–5.0 wt % and a screw speed of 300 rpm [Fig. 9(b,b′)].

CONCLUSIONS

This article provides a comprehensive study of various parameters on PP/clay nanocomposite morphology and their optimization. In this study, the application of response surface methodology, contour plot and Box-Behnken was successfully applied to find out the optimum level of the factors. A quadratic model was obtained using MINITAB-15 software. The variables of model investigated in this study were PP-*g*-MA (wt %) (X_1), clay (wt %) (X_2) and screw speed (rpm) (X_3). The fluorescence spectra showed in fact valuable information on the size and distribution of the filler inside the polymer. Fluorescent probe Nile Blue was used for its sensitivity to their micro and nanostructure environment. An intensity ratio (I_{625}/I_{555}) close to unity showed a better exfoliated morphology. XRD technique and TEM were considered to be complementary to this fluorescence spectroscopy. It is observed that, higher content of PP-*g*-MA leads to better exfoliation and a corresponding increase in reinforcement upto a certain level.

The author thanks Dr. Siddharth Pandey of Indian Institute of Technology Delhi for his cooperation regarding fluorescence spectroscopic analysis.

References

1. Chen, B.; Evans, J. R. G.; Greenwell, H. C.; Boulet, P.; Coveney, P. V.; Bowden, A. A.; Whiting, A. Chem Soc Rev 2008, 37, 568.
2. Paul, D. R.; Robeson, L. M. Polymer 2008, 49, 3187.
3. Alexandre, M.; Dubois, P. Mater Sci Eng 2000, 28, 1.

4. Liu, X.; Wu, Q. Polymer 2001, 42, 10013.
5. Wang, Y.; Chen, F. B.; Wu, K. C. J Appl Polym Sci 2005, 97, 1667.
6. Treece, M. A.; Zhang, W.; Moffitt, R. D.; Oberhauser, J. P. Polym Eng Sci 2007, 47, 898.
7. Wang, Y.; Chen, F. B.; Wu, K. C. J Appl Polym Sci 2004, 93, 100.
8. Myers, R. H.; Montgomery, D. C. Response Surface Methodology; Wiley: New York, 2002.
9. Charles, R. H.; Kennneth, V. T., Jr. Fundamental Concepts in the Design of Experiments; University Press: Oxford, 1999.
10. Box, G. E. P.; Hunter, W. G.; Hunter, J. S. Statistics for Experiments—An Introduction to Design, Data Analysis and Model Building; Wiley: New York, 1978.
11. Abbasi, A. F.; Ahmad, M.; Wasim, M. ACI Mater J 1987, 84, 55.
12. Zhang, Y. P.; Zhang, Y. J.; Gong, W. J.; Wang, S. M.; Xue, H. Y.; Lee, K. P. J Liq Chromatogr Relat Technol 2007, 30, 215.
13. Lahlali, R.; Massart, S.; Najib, S. M.; Jijakli M. H. Int J Food Microbiol 2008, 122, 100.
14. Martendal, E., Budziak, D.; Carasek, E. J Chromatogr A 2007, 1148, 131.
15. Chopra, S.; Motwani, S. K.; Iqbal, Z.; Talegaonkar, S.; Ahmad, F. J.; Khar, R. K. Eur J Pharm Biopharm 2007, 67, 120.
16. Das, A.; Ishtiaque, S. M.; Niyogi, R. Textile Res J 2006, 76, 913.
17. Nouri, M.; Morshedian, J.; Rabbani, A.; Ghasemi, I.; Ebrahimi, M. Iran Polym J 2006, 15, 155.
18. Ng, K. C.; Kadirgama, K.; Ng, E. Y. K. Energy Buildings 2008, 40, 774.
19. Evans, M. Optimization of Manufacturing Processes: A Response Surface Approach; Carlton House Terrace: London, 2003.
20. Ogawa, M.; Kuroda, K. Chem Rev 1995, 95, 399.
21. Maupin, P. H.; Gilman, J. W.; Harris, R. H.; Bellaye, S.; Bur, A. J.; Roth, S. C.; Murariu, M.; Morgan, A. B.; Harris, J. D.; Macromol Rapid Commun 2004, 25, 788.
22. Aloisi, G.; Costantino, U.; Latterini, L.; Nocchetti, M.; Camino, G.; Frache, A. J Phys Chem Solids 2006, 67, 909.
23. Aloisi, G.; Coletti, N.; Costantino, U.; Elisei, F.; Nocchetti, M. Langmuir 1999, 15, 4454.
24. Aloisi, G.; Coletti, N.; Costantino, U.; Elisei, F.; Latterini, L.; Nocchetti, M. Langmuir 2000, 16, 10351.
25. Aloisi, G.; Costantino, U.; Elisei, F.; Nocchetti, M.; Sulli, C. Mol Cryst Liq Cryst 1998, 311, 245.
26. Aloisi, G.; Costantino, U.; Elisei, F.; Latterini, L.; Nocchetti, M. Phys Chem Chem Phys 2002, 4, 2792.
27. Kelly, P.; Akelah, A.; Qutubuddin, S.; Moet, A. J Mater Sci 1994, 29, 2274.
28. Kojima, Y.; Fujushima, A.; Usuki, A.; Okada, A.; Kurauchi T. J Mater Sci Lett 1993, 12, 889.
29. Giannelis, E. P. Adv Mater 1996, 8, 29.
30. Banerjee, S.; Joshi, M.; Ghosh, A. K. Polym Compos 2007 2010, 31.
31. Gopal, M.; Pakshirajan, K.; Swaminathan, T. Appl Biochem Biotechnol 2002, 102, 227.
32. Brown, B. W. Am Mineral 1949, 34, 98.
33. Pattanayak, A.; Jana, S. C. Polymer 2005, 46, 3394.
34. Osman, M. A.; Rupp, J. E. P.; Suter, U. W. Polymer 2005, 46, 1653.
35. Liu, T.; Phang, I. Y.; Shen, L.; Chow, S. Y.; Zhang, W. D. Macromolecules 2004, 37, 7214.
36. Qu, X.; Guan, T.; Liu, G.; She, Q.; Zhang, L. J Appl Polym Sci 2005, 97, 348.
37. Yoon, P. J.; Hunter, D. L.; Paul, D. R. Polymer 2003, 44, 5323.
38. Tjong, S. C. Mater Sci Eng 2006, 53, 73.